

NICMOS Camera 2 Coronagraphic ACQs

A.B. Schultz, K. Noll, A. Storrs, J. Bacinski, W. Baggett, and D. Fraquelli
May 29, 1998

ABSTRACT

The NICMOS Camera 2 coronagraphic target acquisition capability (mode: ACQ) was successfully tested on 1998 February 6. The scheduling and execution of coronagraphic programs was started during February 1998. The NICMOS target acquisition allows the user to acquire a point source and position it into the coronagraphic hole. We are monitoring the coronagraphic programs to search for any potential problems that could impact the success or failure of the ACQs. We have evaluated 38 Camera 2 on-board ACQs, and describe in this report the stability of coronagraphic target acquisitions. The repeatability of the ACQ to position a target at the coronagraphic aperture (NIC2-CORON) reference point is extremely good.

1. Introduction

The Near Infrared Camera and Multi-Object Spectrometer (NICMOS) is a second generation Hubble Space Telescope (HST) instrument. The hole in the Camera 2 Field Divider Assembly (FDA) mirror face, combined with a cold mask, provides coronagraphic imaging capability in Camera 2 (NIC2). The useful radius of the coronagraphic hole is ~ 0.4 arcsec. In the standard on-board acquisition procedure, a target is imaged in a region of NIC2 near the hole, centroiding (to determine the target's position) is performed, offsets are automatically calculated, and the telescope is commanded to slew to position the hole at the location of the target. This procedure is generally specified by a single Phase II exposure line using ACQ mode.

An image of a star is formed on the Field Divider Assembly (FDA) and the hole is on the FDA. Thus, the image on the detector of a star in the hole will still have diffraction spikes. The hole traps the light from the core of the PSF, reducing the diffracted energy outside of the hole by reducing the high frequency components in the PSF. Thus, the light scattering downstream of the FDA is greatly reduced. Some ringing in the image is introduced due to combining the edge effects from the hole on top of the stellar PSF.

The goals of the NIC2 coronagraphic acquisition monitoring program are to track the success and failure rate of acquiring targets, evaluate the stability and repeatability of positioning of a target at the coronagraphic aperture (NIC2-CORON) reference point, and to provide to observers recommendations to achieve the best possible science from their coronagraphic observations.

An in-depth description of NICMOS can be found in the NICMOS Instrument Handbook, Version 2.0, July 1997. The Phase II procedures for specifying a NICMOS ACQ using the flight software and for Mode 1 acquisitions of bright targets can be found in NICMOS ISR-31 “NICMOS Camera 2 Coronagraphic Acquisition”.

2. Overview of NIC2 ACQs

During Science Mission Orbital Verification (SMOV), it was determined that decentering a point source by a small amount, $x=-0.75$, $y=-0.25$ pixels, from the center of the hole reduced the background intensity (program ID: 7052, see NICMOS IDT report “Results from SMOV 7052 NICMOS Coronagraphic Performance Verification”). Based on the SMOV results, this offset has been implemented in the NICMOS ACQ flight software.

The NICMOS dewar anomaly has caused the coronagraphic hole to migrate to different locations on the detector. The position of the hole on the detector can move ~ 0.25 pixel in three orbits. This movement forces a remeasurement of the hole’s coordinates when acquiring a target in the coronagraphic mode. A target must be positioned in the hole to a fraction of a pixel to minimize PSF diffraction and scattered light. Therefore, the precise location of the coronagraphic hole is needed to achieve coronagraphic imaging, requiring a determination of the hole location for each NICMOS ACQ.

The location of the coronagraphic hole is determined from pointed flat field observations. Two short ACCUM F160W filter exposures (7.514 seconds each) with calibration Lamp 1 on (flat field) and two identical exposures with the lamp off (background) are obtained before the acquisition image. The flight software (FSW) combines the two background and two flat field images by performing a pixel-by-pixel minimum to eliminate cosmic rays (using the lower valued pixel of the two frames). The processed background is subtracted from the processed lamp flat. A small 32×32 pixel subarray containing the hole is extracted and a small checkbox (7×7 pixels) is used to find the location with the minimum total counts. Once the minimum checkbox sum is located, a weighted moment algorithm is applied to determine the flux-weighted centroid within the checkbox. The location of the hole is temporarily stored onboard, but it is not included in the science telemetry.

The acquisition image of the target is specified on the Phase II exposure line by the user and any filter or ACQ exposure time can be used to image the target. The target is positioned within a square area 128×128 pixels aperture (center at 157,128). Two

ACCUM images of equal exposure are obtained. The two images are pixel-by-pixel minimized to eliminate cosmic ray hits and a constant value (data negative limit) is added to the processed image. The brightest point source in the acquisition aperture is determined by summing the counts in a checkbox of size 3x3 detector pixels. The algorithm passes the checkbox over the entire acquisition aperture. The brightest checkbox is selected and the location of the target is determined by centroiding the X,Y center of the 3x3 checkbox.

The location of the target and the slew are saved, and are contained in the embedded engineering attached to the following science observation. These values are recovered from the embedded engineering and written to keywords (NXCENT,NYCENY,NOFFSETX,NOFFSETY) in the SPT file. A description of the SPT file can be found in the HST Data Handbook. These header keyword values are not in detector coordinates and must be converted. As presented, they are currently useless to the observer. In the next section, an example of how to convert these values into detector coordinates will be presented.

New coronagraphic keywords (NXCENTP,NYCENY,NOFFSETXP,NOFFSETYP) will be added to the SPT file. These new keywords will contain the target location and slew values converted to pixels. However, the expected time for inclusion of these new keywords in the SPT file is sometime in 1999 and will not be available to NICMOS coronagraphic observers during Cycle 7.

The flight software processed images are not saved, but the two background, two flat field, and two acquisition ACCUM images are sent to the ground. These images, which are executed in a single target acquisition observation, have been packaged into one data set with the same rootname (ippssoot) but with different extensions. Table 1 lists the file name for the NICMOS ACQ data set. These images are written to the distribution tape sent to the PI. A complete description of NICMOS data sets, file format, and header keywords can be found in the HST Data Handbook, Version 3, October 1997.

Table 1. ACQ data image extensions

Extension	Image Contents
ippssoot_raw	Raw target data
ippssoot_rwb	Raw background data
ippssoot_rwf	Raw flat field data
ippssoot_spt	Target SHP and UDL information
ippssoot_spb	Background SHP and UDL information
ippssoot_spt	Flat field SHP and UDL information
ippssoot_cal	Calibrated target data
ippssoot_clb	Calibrated background data

Extension	Image Contents
ippssoot_clf	Calibrated flat field data
ippssoot_trl	OPUS processing trailer file
ippssoot_pdq	OPUS Processing Data Quality file

The NICMOS ACQ ACCUM observations are not completely calibrated. There are no DARK calibration images in OPUS to support ACQ ACCUM observations. This calibration step is skipped when the ACCUM observations are calibrated in OPUS. There are no plans to obtain DARK observations for these data as each observer could specify different exposure times. However, the NICMOS Instrument Definition Team (IDT) is obtaining a few DARK observations in support of their ACQ observations. DARKs are considered calibrations and have no propriety period and can be retrieved from the HST Archive.

3. FSW determined location of the coronagraphic hole and target

The location of the coronagraphic hole is determined by centroiding the X,Y center of the checkbox with the least counts, while the location of the target is determined by centroiding the X,Y center of the brightest checkbox. The algorithm used was borrowed from the IRAF task **imcentroid**. This algorithm was developed by Ball Aerospace for on-board Target Acquisitions (TAs). The spacecraft slew to move the telescope and position the coronagraphic hole reference point at the star location is the difference between the X,Y (hole) and the X,Y (target). The desired total error budget is $\sim 1/12$ pixel (~ 0.007 arcsec) or less.

The target location (NXCENT, NYCENT) and slew (NOFFSETX, NOFFSETY) values are recovered from the telemetry and written to keywords in the SPT file. The first observation following the NICMOS ACQ will contain the updated values. The target location and slew values of the most recent target acquisition will be reflected in following observations until the next acquisition executes, or until the values are re-initialized to zero. These values are not initialized during normal operation of NICMOS.

The IMAGE coordinate systems for NICMOS Cameras 1, 2, 3 have been defined such that the origin will be in the lower left hand corner when displayed, while detector coordinates (DEC) are defined by the readout directions for each camera. Any NICMOS camera image when displayed using the IRAF **display** command will be displayed relative to the HST Field of View (FOV) as depicted in the NICMOS Instrument Handbook. The conversion from detector coordinates to IMAGE coordinates is performed during OPUS pipeline processing. For Camera 2, the OPUS +x direction is detector -y direction, and correspondingly, the OPUS +y direction is detector -x direction. Care must be exercised when converting from one coordinate system to the other.

The target position coordinates are converted into detector coordinates by dividing by 256. However, the slew values are written in 2's compliment. A value less than 32757 is positive, while a value larger than 32757 is negative. Slew values need to be divided by 128 during the conversion into detector coordinates. For example, the following target and slew values were obtained from an SPT file and converted to detector coordinates.

```
> hedit n4q832nrq_spt.fits[1] NXCENT,NYCENT,NOFFSETX,NOFFSETY .
n4q832nrq_spt.fits[1],NXCENT = 31418
n4q832nrq_spt.fits[1],NYCENT = 20655
n4q832nrq_spt.fits[1],NOFFSETX = 10101
n4q832nrq_spt.fits[1],NOFFSETY = 52259
```

```
NXCENT = 31418.0 / 256.0 = 122.726
NYCENT = 20655.0 / 256.0 = 80.683
```

```
NOFFSETX = 10101.0 / 128.0 = 78.914
NOFFSETY = (52259.0 - 65535.0) / 128.0 = -103.718
```

The position of the coronagraphic hole is not saved, but can be inferred by subtracting the offset slew and the coronagraphic hole offset from the position of the target.

```
NXCENT = 122.726 - 78.914 - 0.25 = 43.562
NYCENT = 80.683 + 103.718 - 0.75 = 183.651
```

There is a flip and sign change in the x- and y-axis between detector coordinates and the coordinates of the OPUS formatted image. The flight software target and hole locations are presented in Tables 2 and 3 respectively.

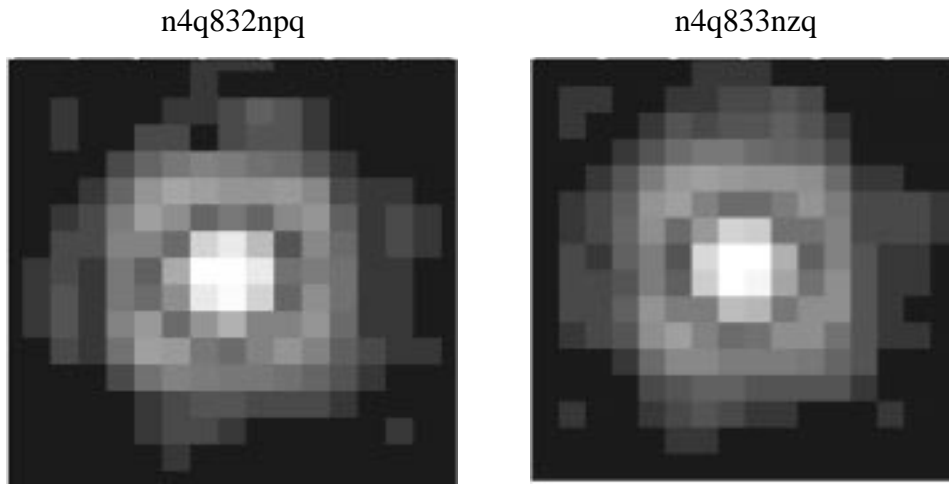


Figure 1: Acquisition images of the same target, identical exposure times and filter. For the first image (left) the peak of the PSF is offset to the left and below the center of the peak pixel, and for the second image (right), the peak of the PSF is offset to the right and below the center of the peak pixel.

The on-board ACQ software locates the 3x3 checkbox with the highest total counts. The centroid task uses a weighted moment centroid algorithm to determine the x and y

position of the PSF in the 3x3 checkbox. For example, the same target was acquired with two acquisitions, n4q832npq and n4q833nzq. The ACQ images for this target are presented in Figure 1. The pixel values for the two acquisition images are presented below. For illustration only, a 3x3 box is drawn about the peak pixel to represent the 3x3 checkbox used by the flight software to centroid the target.

n4q832npq					
	174	175	176	177	178
136	1195.43	550.90	771.39	473.10	1142.60
135	632.89	5123.24	8025.74	3487.81	301.34
134	2343.82	12761.57	17934.81	8524.96	679.30
133	1298.38	8843.01	12434.98	5338.02	540.76
132	570.98	1433.19	2548.74	1016.13	999.86

n4q833nzq					
	172	173	174	175	176
129	1865.65	978.28	652.82	628.16	909.31
128	617.25	1624.43	5510.08	4674.90	734.68
127	342.41	6025.60	15543.21	12805.26	2767.10
126	391.54	4922.07	13271.35	10714.96	2236.92
125	896.62	940.20	3431.26	2941.97	852.17

For the first ACQ image (n4q832npq), the peak of the PSF is offset to the left and below the center of the peak pixel, while for the second ACQ image (n4q833nzq), the peak of the PSF is offset to the right and below the center of the peak pixel.

4. IRAF determined location of the target position

The NICMOS detectors are 256x256 pixel arrays of HgCdTe (mercury-cadmium-telluride) photodiodes. Each pixel is individually bump-bonded to a single pixel of a silicon multiplexer which is used as a readout. The pixel elements are on 40 micron centers, center-to-center. There is a space between each pixel of lower sensitivity which defines a pixel boundary, making each pixel independent of other pixels. Each pixel element is ~38 microns on a side with a space between pixels of about 1 to 2 microns. Each quadrant of the array is read out separately, a row at a time. All the pixels from the 128 pixel row are sequentially A/D converted as fast as the A/D converter will allow. The readout multiplexer and column indexer can scan faster than the A/D can convert. Thus, a single pixel

can be selected and converted by the clocking sequence. The above is noted here for observers using BRIGHT OBJECT Mode.

The flux from a stellar PSF will be shared by adjacent pixels. The brightest pixel of an image will depend upon where the PSF falls on the array. If a stellar PSF does not fall at the center of a pixel, energy will fall between the pixels and the PSF centroid can be uncertain up to $\sim 1/2$ pixel. For Camera 2, the pixel size is 75 mas. For a Camera 2 PSF, $\sim 90\%$ of the energy in the J, H, and K bands (1.25, 1.65, and 2.22 microns) will be contained within radii of 230, 300, 400 mas (~ 3 , ~ 4 , and ~ 5 pixels respectively). The location of the stellar PSF on the detector should not result in a large error in determining the centroid or in the resulting slew.

The location of the target is saved, and IRAF can be used to check the FSW position. The IRAF task **center** can be used to determine the centroid of the target in the NIC2 Field of View (FOV). For the following **center** examples, the “centroid” centering algorithm was used with a cbox = 5.0 pixels to determine the centroid of the target and the hole.

```
> center n4q832npq_cal.fits[sci,1] coord=target.lis out=target.da
```

Once the IRAF positions of the target have been determined, the values need to be converted into detector coordinates by subtracting them from 256.5. For example:

```
star      NYCENTER = 256.5 - 175.708 = 80.792  
          NXCENTER = 256.5 - 133.725 = 122.775
```

The positions of targets as determined by the FSW and from the on-board ACQ images as determined with IRAF are presented in Table 2.

A comparison between the FSW and IRAF determined positions of the targets (35 data points) listed in Table 2 shows a mean difference of -0.008 ± 0.030 pixels for the x-position and a mean difference of -0.005 ± 0.039 pixels for the y-position. The IRAF determined target positions listed in Table 2 agree quite well with the FSW determined target positions. The slight differences are most probably due to the different algorithms used to determine the centroids. Any error in positioning a target at the scatter offset point in the coronagraphic hole is not in the FSW target location algorithm.

For example, an anomalous displacement of ~ 1.15 pixels at the coronagraphic hole was measured for back-to-back observations of the same target (n4q832npq, n4q833nzq). The ACQs were separated by 30 minutes. This difference is quite large and almost 4 times the maximum range for other targets observed in a similar manner. From above, we can eliminate the FSW algorithm for determining the location of the target as the possible source of the positional error.

In the Section 6, we perform the same analysis for determining the hole position.

Table 2. Locations of the target. Measurements determined from NICMOS ACQ data sets, Flight Software (FSW) and IRAF in detector coordinates (DEC). The coordinates are presented in detector coordinates (DEC).

Prop.ID (visit)	FSW-Target Location		IRAF-Target Location	
	X-center (pixel)	Y-center (pixel)	X-center (pixel)	Y-center (pixel)
7226 (03)	126.570	99.421	126.622	99.378
7226 (04)	125.371	95.804	125.308	95.832
7226 (13)	140.707	117.250	140.738	117.220
7226 (14)	124.164	112.710	124.162	112.733
7226 (57)	154.968	134.183	154.983	134.165
7226 (58)	136.539	144.136	136.580	144.134
7226 (61)	157.574	119.890	157.623	119.899
7226 (62)	144.007	125.101	144.004	125.102
7227 (07)	137.871	92.917	137.887	92.922
7227 (08)	143.800	94.972	143.819	94.971
7227 (17)	132.363	121.636	132.353	121.670
7227 (18)	124.574	109.406	124.615	109.354
7227 (45)	144.160	135.812	144.143	135.845
7227 (46)	123.546	123.808	123.500	123.815
7227 (49)	132.738	84.531	132.759	84.533
7227 (50)	133.792	81.675	133.811	81.711
7227 (57)	143.757	112.128	143.803	112.106
7227 (58)	140.187	121.910	140.176	121.919
7227 (59)	140.113	82.503	140.100	82.505
7227 (60)	141.062	75.671	141.057	75.719
7233 (05)	127.996	82.179	127.982	82.127
7233 (06)	130.109	86.457	130.089	86.442
7233 (13)	130.296	96.691	130.278	96.735
7233 (32)	122.726	80.683	122.775	80.792
7233 (33)	129.882	82.144	129.902	82.103
7329 (61)	120.207	97.277	120.193	97.261
7329 (81)*	181.984	138.441	-	-

Prop.ID (visit)	FSW-Target Location		IRAF-Target Location	
	X-center (pixel)	Y-center (pixel)	X-center (pixel)	Y-center (pixel)
7329 (86)*	181.980	138.531	163.662	85.154
7418 (04)	137.003	94.949	137.008	94.954
7834 (03)	145.136	113.628	145.164	113.683
7834 (05)	134.050	101.960	134.068	101.976
7834 (08)	144.992	103.843	144.964	103.802
7834 (09)*	140.019	114.218	-	-
7834 (12)	140.378	105.539	140.387	105.549
7857 (03)	127.816	92.535	127.853	92.457
7857 (a3)	138.929	97.785	138.938	97.811
7897 (21)	129.757	95.855	129.811	95.895
7897 (59)	131.679	89.726	131.752	89.818

Note: * - failed acquisitions, no target found.

5. NICMOS acquisition anomalies

Even though a target was in the NICMOS Camera 2 FOV at pixel location (163.662, 85.154), the flight software did not find the target for program 7329 visit 86. The detected counts for this target were low. The flight software centered up on noise, a bright pixel at location (181.980, 138.531). This is a SNAP shot program and a fraction of the targets are expected to be missed.

Two coronagraphic ACQs failed due to no target in the NICMOS Camera 2 FOV, programs 7329 visit 81 and 7834 visit 09. Again, the FSW centered up on noise.

6. IRAF determined location of the coronagraphic hole

The coronagraphic hole location determined from off-line processed ACQ images should be very close to the inferred location of the hole determined by subtracting the FSW slew from the FSW target position. However, the hole pattern is not symmetric about the low scatter point (pixel with least counts) of the OPUS pipeline processed coronagraphic hole image due to the impression of the flat field on top of the image. The on-board ACQ background and flat field images need to be reduced in a similar manner as performed by the FSW to achieve a meaningful comparison. The coronagraphic acquisition discussed in the previous section, n4q832npq, will be used as an example to demonstrate manually off-line processing.

The background image (n4q832npq_rwb.fits) must be subtracted from the image of the hole (n4q832npq_rwf.fits) and the resulting image flat fielded using a preflight flat or SMOV flat with the hole at a different position. For the example, the pre-flight flat field h1s1337dn_ft.fits was used to process the hole image. The IRAF tasks **imcalc** and **imarith** were used to process the hole image. The task **imcalc** was used to perform a pixel-by-pixel minimization to eliminate cosmic rays.

```
> imcalc n4q832npq_rwb01.fits[1],n4q832npq_rwb02.fits[1] min_bac
"min(im1,im2)"

> imcalc n4q832npq_rwf01.fits[1],n4q832npq_rwf02.fits[1] min_flat
"min(im1,im2)"

> imarith min_flat.hhh - min_bac.hhh min_flat_bac
> imarith min_flat_bac.hhh * nref$h1s1337dn_ft.fits[1] pro_flat_bac
```

While the FSW finds a minimum, we invert the flat field image to make the hole positive and use the IRAF task **center** to determine the centroid of the reversed hole image. For example:

```
> imarith 5500.0 - pro_flat_bac.hhh diff_flat_bac.hhh
> center diff_flat_bac.hhh coord=hole.lis out=hole.da
```

The position of the coronagraphic hole measured from the pipeline processed image is (73.384, 213.082), while the measured position of the hole from the off-line processed image is (73.273, 213.163). The difference is ~0.1 pixel in the x- and y-positions. This measured offset in hole position is most probably due to the different calibrations performed on the ACQ images. The pipeline processed ACCUM images are not dark or background corrected and the location of the coronagraphic hole in the pipeline on-orbit flat is patched.

Once the IRAF positions of the hole have been determined, the values need to be converted into detector coordinates by subtracting them from 256.5. For example:

```
hole    NYCENTER = 256.5 - 73.273 = 183.227
        NXCENTER = 256.5 - 213.163 = 43.337
```

For images n4q832npq and n4q833nzq, the difference between the two positions of the hole (IRAF and FSW) in detector coordinates is ~0.9 pixels in the y-position and ~0.3 pixels in the x-position. This difference in position is much larger than can be explained by summing the errors in quadrature (square root of the sum of the errors squared). The pipeline and off-line processed images of the coronagraphic hole for observation n4q832npq are presented in Figure 2.

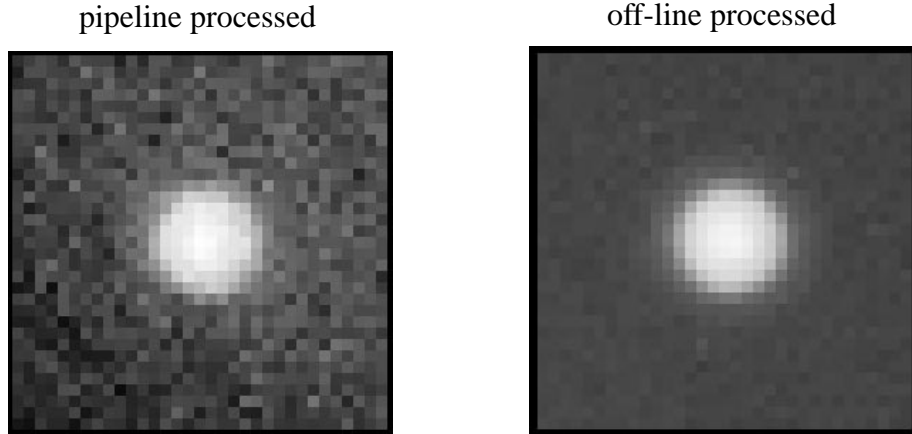


Figure 2: Image of coronagraphic hole. A 32x32 pixel area centered on the coronagraphic hole. Images extracted from on-board F160W flat field observation n4q832npq. Pipeline processed (left), and off-line processed (right) in a similar manner as performed by the FSW. Images inverted to show detail about the hole.

The inferred location of the coronagraphic hole by subtracting the FSW slew from the FSW target position for the two acquisitions (n4q832npq, n4q833nzq) shows a jump of ~ 1 pixel in the x position of the hole compared to other FSW inferred locations for the hole. In addition, there is a ~ 1.4 pixel shift in the inferred y position of the hole between the two ACQs. A total shift for the hole location of ~ 0.16 pixel was measured between the two flat field observations using IRAF.

The FSW inferred positions of the coronagraphic hole and the hole positions determined from off-line processed images are presented in Table 3.

Table 3. Locations of the coronagraphic hole. Measurements determined from off-line processing of NICMOS ACQ data sets, Flight Software (FSW) and IRAF in detector coordinates (DEC). The coordinates are presented in detector coordinates (DEC).

Prop.ID (visit)	FSW-Hole Location		IRAF Hole Location	
	X-center (pixel)	Y-center (pixel)	X-center (pixel)	Y-center (pixel)
7226 (03)	43.469	183.577	43.566	183.389
7226 (04)	43.481	183.585	43.473	183.361
7226 (13)	43.356	183.429	43.839	183.697
7226 (14)	43.360	183.452	43.756	183.642

Prop.ID (visit)	FSW-Hole Location		IRAF Hole Location	
	X-center (pixel)	Y-center (pixel)	X-center (pixel)	Y-center (pixel)
7226 (57)	43.398	183.472	43.717	183.557
7226 (58)	43.407	183.495	43.754	183.496
7226 (61)	44.676	183.319	44.025	183.906
7226 (62)	43.289	183.335	43.987	183.915
7227 (07)	43.489	183.581	43.504	183.373
7227 (08)	43.472	183.573	43.524	183.380
7227 (17)	43.442	183.643	43.578	183.261
7227 (18)	43.449	183.656	43.585	183.198
7227 (45)	44.637	183.272	44.169	183.719
7227 (46)	44.648	183.300	44.049	183.987
7227 (49)	44.582	183.296	44.258	183.994
7227 (50)	44.589	183.307	44.249	184.002
7227 (57)	43.437	183.534	43.599	183.441
7227 (58)	43.445	183.558	43.597	183.421
7227 (59)	43.293	183.346	43.969	183.858
7227 (60)	43.296	183.358	43.954	183.861
7233 (05)	44.684	183.359	44.007	183.906
7233 (06)	44.680	183.355	44.023	183.806
7233 (13)	43.375	183.464	43.799	183.635
7233 (32)	43.562	183.651	43.337	183.227
7233 (33)	43.562	182.253	43.256	183.085
7329 (61)	43.473	183.581	43.536	183.389
7329 (81)	43.313	183.370	43.952	183.657
7329 (86)	43.363	183.437	43.852	183.657
7418 (04)	43.394	183.652	43.750	183.240
7834 (03)	44.652	183.362	44.099	183.877
7834 (05)	43.355	183.616	43.841	183.282
7834 (08)	43.485	183.593	43.556	183.285
7834 (09)	44.598	183.288	44.257	183.987
7834 (12)	43.410	183.492	43.667	183.506

Prop.ID (visit)	FSW-Hole Location		IRAF Hole Location	
	X-center (pixel)	Y-center (pixel)	X-center (pixel)	Y-center (pixel)
7857 (03)	43.449	182.261	43.574	183.123
7857 (a3)	43.453	182.253	43.538	183.114
7897 (21)	42.312	182.581	42.785	182.281
7897 (59)	43.351	183.405	43.849	183.758

A comparison between the FSW and IRAF determined positions of the coronagraphic hole is presented graphically in Figure 3. The FSW inferred positions of the coronagraphic hole show a correlated movement over time in the location of the hole and groups of outlier points that exhibit a ~ 1 pixel jump in the x- or y-positions of the hole. The IRAF determined positions of the hole also shows a correlated movement in the hole position over time as well as some scatter about the movement line, but no large 1 pixel jumps in the position of the hole.

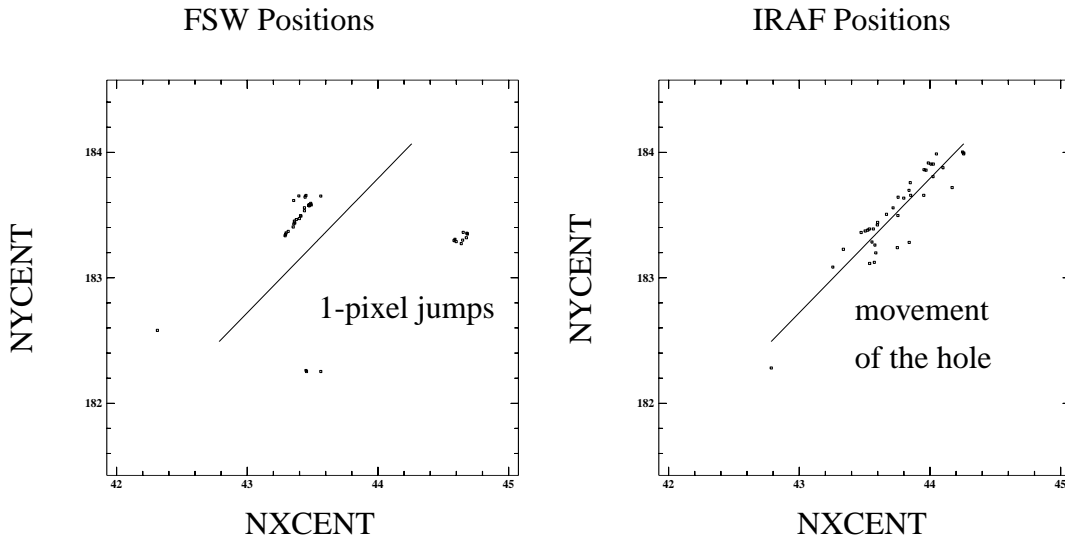


Figure 3: Coronagraphic hole locations. Flight Software (FSW) inferred hole positions (left), and IRAF determined hole positions (right). Outlier points in the FSW plot are due to anomalous 1 pixel jumps in the inferred position of the hole. The movement in the position of the hole over time is evident in the IRAF plot and is represented by the line in both plots.

Excluding the 12 observations that exhibit a 1-pixel jump, the mean difference between the FSW inferred position of the coronagraphic hole and the IRAF determined

position of the hole is -0.30 ± 0.24 pixels in the x-position and 0.02 ± 0.30 pixels in the y-position, yielding a total mean difference of 0.44 ± 0.21 pixels. The differences are presented in Table 4.

Table 4. Coronagraphic hole position differences. Differences between the Flight Software (FSW) positions and the IRAF determined positions from off-line processed NICMOS ACQ data sets. The differences are presented in detector coordinates (DEC).

	FSW-IRAF Location	FSW-IRAF Location	Hole Location
Prop.ID (visit)	delta-X (pixel)	delta-Y (pixel)	Difference (pixel)
7226 (03)	-0.097	0.188	0.211
7226 (04)	0.008	0.224	0.224
7226 (13)	-0.483	-0.268	0.552
7226 (14)	-0.396	-0.190	0.439
7226 (57)	-0.319	-0.085	0.330
7226 (58)	-0.347	-0.001	0.347
7226 (62)	-0.698	-0.580	0.907
7227 (07)	-0.015	0.208	0.208
7227 (08)	-0.052	0.193	0.199
7227 (17)	-0.136	0.382	0.405
7227 (18)	-0.136	0.458	0.477
7227 (57)	-0.162	0.093	0.186
7227 (58)	-0.152	0.137	0.204
7227 (59)	-0.676	-0.512	0.848
7227 (60)	-0.658	-0.503	0.828
7233 (13)	-0.424	-0.171	0.457
7233 (32)	0.225	0.424	0.480
7329 (61)	-0.063	0.192	0.202
7329 (81)	-0.639	-0.2871	0.700
7329 (86)	-0.489	-0.220	0.536
7418 (04)	-0.356	0.412	0.544
7834 (05)	-0.486	0.334	0.589
7834 (08)	-0.071	0.308	0.316

	FSW-IRAF Location	FSW-IRAF Location	Hole Location
Prop.ID (visit)	delta-X (pixel)	delta-Y (pixel)	Difference (pixel)
7834 (12)	-0.257	-0.014	0.257
7897 (21)	-0.473	0.300	0.560
7897 (59)	-0.498	-0.353	0.610

7. Back-to-back ACQ observations

The NICMOS dewar anomaly has caused the coronagraphic hole to migrate to different locations on the detector. The position of the hole on the detector can move ~ 0.25 pixel in three orbits. This movement requires that the hole location be determined for each coronagraphic observation. A few Cycle 7 NICMOS coronagraphic programs (7226, 7227, 7233) are acquiring the same target twice during the same orbit with different spacecraft rolls by the use of two 1/2 orbit visits. This technique is a limited resource and must be pre-approved before implementation. Twelve of these visits have been reviewed for this report.

The FSW position of the hole is temporarily stored on-board and is not written to the embedded engineering attached to the science data. However, it is captured intermittently in the engineering telemetry. The captured FSW position of the hole agrees with the inferred FSW hole position determined by subtracting the slew from the FSW position of the star. This result indicates the inferred jumps in the hole position are due to a FSW problem. The differences in the inferred FSW hole positions are tabulated in Table 5.

Table 5. FSW coronagraphic hole locations. Inferred hole displacement determined from back-to-back ACQ observations obtained in one orbit. The coordinates are presented in detector coordinates (DEC).

Prod. ID (visit)	X-center (pixel)	Y-center (pixel)	delta-X (pixel)	delta-Y (pixel)	displacement (pixel)
7226 (03)	43.469	183.577			
7226 (04)	43.481	183.585	-0.012	-0.008	0.014
7226 (13)	43.356	183.429			
7226 (14)	43.360	183.452	-0.004	-0.023	0.023
7226 (57)	43.398	183.472			
7226 (58)	43.407	183.495	-0.009	-0.023	0.024
7226 (61)	44.676	183.319			

Prod. ID (visit)	X-center (pixel)	Y-center (pixel)	delta-X (pixel)	delta-Y (pixel)	displacement (pixel)
7226 (62)	43.289	183.335	1.387	-0.016	1.387
7227 (07)	43.489	183.581			
7227 (08)	43.472	183.573	0.017	0.008	0.018
7227 (17)	43.442	183.643			
7227 (18)	43.449	183.656	-0.007	-0.013	0.014
7227 (45)	44.637	183.272			
7227 (46)	44.648	183.300	-0.011	-0.028	0.039
7227 (49)	44.582	183.296			
7227 (50)	44.589	183.307	-0.007	-0.011	0.013
7227 (57)	43.437	183.534			
7227 (58)	43.445	183.558	-0.008	-0.024	0.025
7227 (59)	43.293	183.346			
7227 (60)	43.296	183.358	-0.003	-0.012	0.012
7233 (05)	44.684	183.359			
7233 (06)	44.680	183.355	0.004	0.004	0.006
7233 (32)	43.562	183.651			
7233 (33)	43.562	182.253	0.000	1.398	1.398

Except for programs 7226 (61/62) and 7233 (32/33), the flight software re-determined the hole location for the second ACQ to be within ~ 0.10 pixel or less of the first location. This indicates that the movement of the hole during a single orbit is quite small. This was verified by using IRAF to determine the location of the hole from the ACQ flat field observations. Table 6 presents hole locations as measured using IRAF. The mean measured displacement (movement) of the coronagraphic hole between ACQs is 0.09 ± 0.08 pixels. There is one large excursion of the hole that occurred during program 7227 visit 46. The cause of the excursion is unknown and is under investigation. Dropping this point from the mean, the mean displacement of the hole becomes 0.07 ± 0.04 pixels.

Table 6. Displacement of the coronagraphic hole during one orbit. Measurements determined from off-line processed NICMOS ACQ flat field data obtained at the start and near the middle of an orbit. IRAF was used to determine the displacement of the hole. The coordinates are presented in detector coordinates (DEC).

Prod. ID (visit)	X-center (pixel)	Y-center (pixel)	delta-X (pixel)	delta-Y (pixel)	displacement (pixel)
7226 (03)	43.566	183.389			
7226 (04)	43.473	183.361	0.093	0.028	0.097
7226 (13)	43.839	183.697			
7226 (14)	43.756	183.642	0.083	0.055	0.099
7226 (57)	43.717	183.557			
7226 (58)	43.754	183.496	-0.037	0.061	0.071
7226 (61)	44.025	184.069			
7226 (62)	43.987	183.915	0.038	0.154	0.158
7227 (07)	43.504	183.373			
7227 (08)	43.524	183.380	-0.020	-0.007	0.021
7227 (17)	43.578	183.261			
7227 (18)	43.585	183.198	-0.007	0.063	0.063
7227 (45)	44.169	183.719			
7227 (46)	44.049	183.987	0.120	-0.268	0.293
7227 (49)	44.258	183.994			
7227 (50)	44.249	184.002	0.009	-0.008	0.012
7227 (57)	43.599	183.441			
7227 (58)	43.597	183.421	0.002	0.020	0.020
7227 (59)	43.969	183.858			
7227 (60)	43.954	183.861	0.015	-0.003	0.015
7233 (05)	44.007	183.906			
7233 (06)	44.023	183.806	-0.016	0.100	0.101
7233 (32)	43.337	183.227			
7233 (33)	43.256	183.085	0.081	0.142	0.163

The same data set can be used to assess the repeatability of ACQs to position the same target at the coronagraphic hole reference point ($x=-0.75$, $y=-0.25$ pixels). Measuring the location of the star image on the detector is problematic due to glint about the hole, which is discussed in Section 9. The approach used for this report was to use the outer wings of

the PSF and diffraction spikes to determine the relative shift between two images of the same target while avoiding the region of the image about the coronagraphic hole.

IRAF task `xregister` was used to cross-correlate two images of the same target. The first coronagraphic image in a data set was used as the reference image. Two regions on each side of the star image ([20:55,160:256] [87:122,160:256]) were used for the cross-correlation. Table 7 presents the relative displacement of target stars following ACQs executed in the same orbit.

Table 7. Relative displacement of targets. Measurements determined from pipeline processed NICMOS coronagraphic observations obtained of the same target following two ACQs executed in one orbit. Each row presents data for a different target. The relative shifts are presented in IRAF coordinates (pixels).

Prop. ID (visit)	X-shift (pixel)	Y-shift (pixel)	displacement (pixel)	hole movement (pixel)
7226 (03/04)	-0.0794	-0.0441	0.090	0.097
7226 (13/14)	-0.0621	-0.1782	0.188	0.099
7226 (57/58)	-0.1056	-0.0359	0.111	0.071
7226 (61/62)	0.6479	-0.9227	1.127	0.158
7227 (07/08)	-0.0372	-0.0921	0.099	0.021
7227 (17/18)	-0.0092	-0.0787	0.079	0.063
7227 (45/46)	0.13851	-0.2326	0.271	0.293
7227 (49/50)	-0.0935	-0.0906	0.130	0.012
7227 (57/58)	-0.3217	-0.0064	0.321	0.020
7227 (59/60)	0.03896	-0.2727	0.275	0.015
7233 (05/06)	-0.1340	-0.0283	0.137	0.101
7233 (32/33)	-1.0610	0.2102	1.155	0.163

Except for two anomalous extreme displacements, 7226 (61/62) and 7233 (32/33), the data indicate that a target was repositioned the second time within a range of ~ 0.1 to ~ 0.3 pixels of the first image. For the two exceptions, the guiding was on two star fine lock, the movement of the hole was less than ~ 0.2 pixel, and there is no evidence in the images of a companion whose light could contribute to the displacement. We do not yet know why these jumps occurred.

The FSW tracked the movement of the hole in 4 out of 12 pairs of observations, positioning the target at the new location of the hole. There was a noticeable jump in hole movement during the pair of observations 7227 (45/46), and the FSW tracked this move-

ment. However, for the remaining 8 pairs of observations, the displacement of the target between observations is greater than the movement of the hole.

8. FGS Guiding

Two guide star (GS) guiding is recommended when performing coronagraphic observations. However, drift about a single guide star is small. If we represent the linear motion due to gyro drift around a star as $X = D \sin(at)$, where X equals the linear motion, D the distance from the guide star to the aperture, a the angular gyro drift rate, and t the time since the last FHST update, then for $D = 20$ arcmin (worst case) = 1200 arcsec and $a = 0.001$ arcsec/sec, for one visibility period $t = 50$ min = 3000 sec we get $X = 0.0175$ arcsec or less than 1/4 pixel in Camera 2. For two orbits $t = 146$ min = 8760 sec, $X = 0.051$ arcsec or a little over 2/3 pixel in Camera 2.

The only time gyro drift about a single guide star will become noticeable in one orbit is when performing coronagraphy-- to be conservative one should only do one orbit on single GS when aperture NIC2-CORON is used.

9. Residual hole fabrication debris (glint)

The hole in the NICMOS Camera 2 Field Divider Assembly (FDA) mirror face was machined in a two step process. First, the bore (~0.3 arcsec) through the back of the mirror was stopped ~1 mm from the front surface. The front surface was laser ablated out. This process resulted in debris surrounding the hole which reflect light (facets) and some removal of surface material about the hole. The useful radius is ~0.4 arcsec. The bright reflections from these artifacts from the boring process have been labeled "glint". There is one azimuth region where the glint is brightest, because there are more debris at that edge of the hole. Figure 4 displays enlarged images of the same target outside and positioned within the coronagraphic hole. The bright glint pattern is different from the NICMOS stellar PSF pattern.

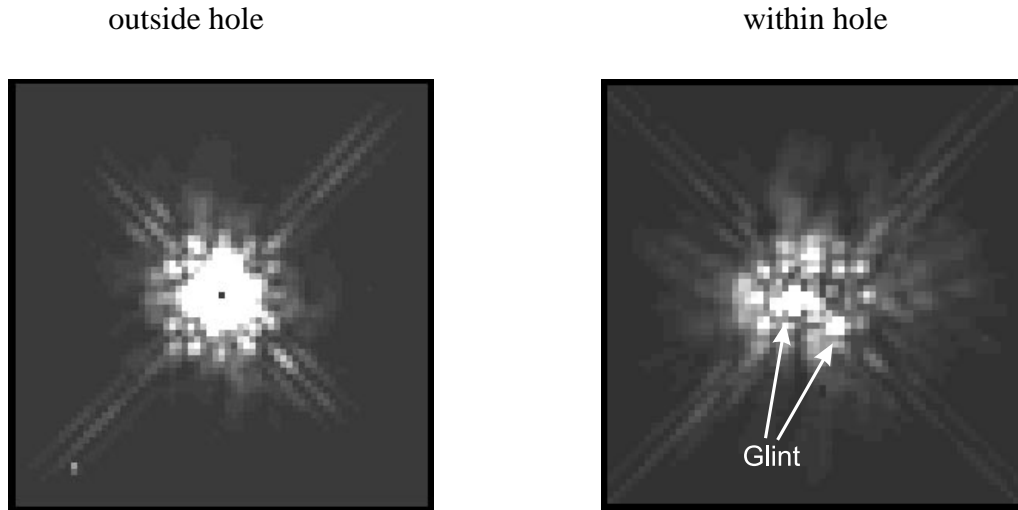


Figure 4: Star images. Star imaged outside the hole (left) and within the coronagraphic hole (right). Images were obtained with the F160W filter. Two bright glint regions are marked with arrows.

10. Conclusions and Recommendations

The Flight Software performed as expected for most of the observations, locating the position of the target and coronagraphic hole, calculating a slew, and positioning the hole over the target (i.e., moving the telescope to put the target into the coronagraphic hole). However, a slight shift between the IRAF and FSW determined positions of the hole indicates a small bias offset of ~ 0.4 pixel in the FSW measured position of the hole. In addition, several observations show a ~ 1 pixel jump in the inferred position of the hole, either in the x- or y-direction. One possibility is a problem in the FSW algorithm to determine the position of the coronagraphic hole. The FSW routines are under review.

The movement of the hole during a single orbit is quite small, less than ~ 0.10 pixel. This has been verified by using IRAF. Back-to-back ACQs of the same target, or possibly of a target star and a PSF reference star, during a single orbit will probably displace the target on the array due to small movements of the hole. This will require a shift of one coronagraphic image to another for PSF subtraction. Perhaps, it would be better to use the hole position found during the first ACQ for a second coronagraphic observation in the same orbit.

Back-to-back coronagraphic observations of the same target performed in the same orbit with a roll between the two ACQs may not provide the desired results for PSF subtraction. Spacecraft breathing will change the focus causing a size induced difference

between the PSF at the start of an orbit and the PSF at the end of an orbit. A better observational method would be to observe the target during identical portions of adjacent orbits, with the observations 96.5 minutes apart. This can be achieved by using the visit level special requirement on the second visit, 'AFTER 01 BY 94 TO 98 M'. A discussion of the effects of spacecraft breathing on NICMOS observations is presented in NICMOS ISR-98-009, "Focus Variation and the Orbital Phase of Observations".

The NICMOS cryogen exhaustion date prediction is currently 1998 December 31 +/- 30 days. Coronagraphic observers should continue to execute their programs even with the possibility of an intermittent 1 pixel jump. Waiting for the FSW to be fixed may result in the observations not being made at all.

11. Recent Caveats

A review of the NICMOS coronagraphic ACQ FSW was performed by Goddard Space Flight Center (GSFC) Code 582 personnel. Their conclusions are that an algorithm enhancement is required and that there was no rounding/truncation problem with the flight software. After discussions with NICMOS IDT, STScI, and Code 582 personnel, it was decided that inverting the on-board flat field before determining the hole position would improve locating the hole position within a 0.2 pixel tolerance. It is expected that new flight software will be delivered during the first week of August 1998.